JOURNAL OF AIRCRAFT
Vol. 35, No. 1, January–February 1998

Boundary Element Analysis of Fatigue Crack Propagation in Stiffened Panels

N. K. Salgado*
Empresa Brasileira de Aeronáutica, S. A., Brazil
and
M. H. Aliabadi†
University of London, Queen Mary College, London, England E1 4NS, United Kingdom

This paper presents the dual boundary element method (DBEM) for the analysis of crack propagation in aircraft-stiffened panels. DBEM can be used to perform mixed mode analysis in panels with single or multiple cracks, stiffened with riveted, bonded, or integral stringers. The stiffeners attachment can be modeled as rigid or flexible with elastic or elastic–plastic behavior. Several examples of stiffened panel problems are presented to demonstrate the accuracy and flexibility of the technique. In one example, the crack growth rates calculated from the stress intensity factors obtained with the method are compared with experimental results and shown to be in good agreement. Another example studies the influence of cracks at adjacent stiffeners on a crack at a central stiffener. The central stiffener can be broken or intact and the adjacent cracks can be aligned with the central crack or not. An example to illustrate the application to multiple site damage problems in fuselage lap joints is also presented.

I. Introduction

AIRWORTHINESS regulations presently require the evaluation of damage tolerance for transport category airframes. An airframe is damage tolerant if it can withstand reasonable loads without catastrophic failure or excessive deformation after the occurrence of serious fatigue damage. Damage tolerance is generally achieved by means of multiple load paths. After the failure of one component, the applied loads are safely distributed to other load-carrying elements.

Stiffened panels are the basic airframe construction cell. The stiffeners can be attached to the sheet by means of fasteners bonded to it or, alternatively, machined to form an integral panel. Riveted and bonded panels are examples of structures with multiple load paths. The stiffeners provide an alternative path to bypass panel load around a cracked skin. If a skin crack reaches a critical length and a skin fracture starts, the load is transferred from the skin to the stiffeners and the fracture is arrested.

Full-scale testing remains the preferred method for demonstrating compliance with damage tolerance requirements. However, it is expensive and time consuming. Numerical analysis based on fracture mechanics theory has been extensively used in the aerospace industry as an alternative to full-scale testing. For practically all of the high-strength materials used in airframes, linear elastic fracture mechanics theory can be applied. The fundamental postulate of linear elastic fracture mechanics states that a parameter called the stress intensity factor, which is a measure of the strength of the stress singularity at a crack tip, can be used to determine the crack behavior. Viegler,[1] Ratwani and Wilhem,[2] Shkarayev and Moyer,[3] among others, showed that the finite element method (FEM) can be used to evaluate stress intensity factors in stiffened panels, and commercial FEM programs are widely used in the aerospace industry.

Great care is required when creating the numerical model. Because of the presence of cracks, the model contains stress singularities at the crack tips. Special crack elements must be employed in the model. The discretization around the crack tips has to be fine, usually requiring a large number of elements. The stiffeners attachment model is also very important for accurate stress intensity factor predictions. Swift[4] demonstrated the importance of taking into account the attachment flexibility. Moreover, when a crack tip is near a stiffener, the attachment forces can reach very high values, leading, eventually, to nonlinear behavior of the connection. Finally, crack growth processes are simulated with an incremental crack-extension analysis. For each increment, the stress intensity factors are calculated and used to predict new crack tip positions. The mesh then needs to be modified to reflect the changes to the crack tip positions. Except for simple mode *I* cases, where the crack trajectory can be predefined, special remeshing strategies are required.

The boundary element method (BEM), has emerged as a powerful numerical technique for fracture mechanics.[5] Its most attractive feature is the reduction of the dimensionality of the numerical model. The high stress gradients near the crack tip can be modeled more accurately and efficiently, in comparison to domain methods such as the FEM, as the necessary concentration of grid points is confined to one less dimension. The dual boundary element method (DBEM), developed by Portela et al.,[6] is capable of analyzing configurations involving any number of edge and embedded cracks in any given geometry under mixed mode load conditions. Furthermore, crack growth problems can be analyzed without any remeshing difficulties.

Dowrick et al.[7] and Young et al.[8] used the BEM to solve problems involving discretely attached, i.e., by means of fasteners, and continuously attached (bonded or integral) stiffeners, respectively. Utukuri and Cartwright[9] and Wu and Cartwright[10] used the boundary collocation method to solve similar problems. Salgado and Aliabadi[11] extended the DBEM to deal with single or multiple crack growth analysis and stiffened panels. Both continuously and discretely attached stiffeners were considered, and the stress intensity factors calculated were shown to be accurate.

In the work presented here, the DBEM and its application to the damage tolerance design of aircraft components is introduced. It will be shown that the method produces accurate predictions for the crack growth life of stiffened panels. Ex-

Received March 16, 1996; revision received Jan. 1, 1997; accepted for publication June 19, 1997.

*Engineer.

†Reader in Aerospace Structures, Department of Engineering.

amples of application are presented, illustrating the ability of the method to solve single or multiple crack problems, under mixed-mode conditions with broken or intact stiffeners, and using rigid or flexible attachments with elastic or elastic–plastic behavior. Finally, one example featuring a multiple site damage (MSD) problem in a fuselage lap joint is presented.

II. DBEM Method for Stiffened Sheets

The basic formulation for the DBEM method will be presented in the following sections. The Cartesian tensor notation is used and Einstein's summation convention adopted. The partial derivative with respect to the Cartesian coordinate x_i is denoted by the comma abbreviation, i.e., $\partial/\partial x_i(\ldots) = (\ldots)_{,i}$.

A. Continuously Attached Stiffeners

Figure 1 presents a cracked sheet with stiffeners continuously bonded to it at n lines inside its domain Ω. When this configuration is subjected to a set of boundary loads and displacement constraints applied at the boundary Γ, the sheet and the stiffeners will deform and share interaction forces over the stiffeners loci L_n. The displacement of a point x' inside the sheet domain Ω is given by

$$u_j(x') = -\int_\Gamma T_{ij}(x', x)u_j(x)\,d\Gamma(x) + \int_\Gamma U_{ij}(x', x)t_j(x)\,d\Gamma(x) + \sum_n \int_{L_n} U_{ij}(x', X)f_j^n(X)\,dL_n(X) \tag{1}$$

where $u_j(x)$ and $t_j(x)$ are unknown displacements and tractions at boundary points x, and $f_j^n(X)$ are the unknown interaction forces. The terms $U_{ij}(x', x)$ and $T_{ij}(x', x)$ are known functions called displacement and traction fundamental solutions, respectively.

If, instead of inside the domain, the point x' is on the boundary Γ, its displacement is given by

$$c_{ij}(x')u_j(x') = -\int_\Gamma T_{ij}(x', x)u_j(x)\,d\Gamma(x) + \int_\Gamma U_{ij}(x', x)t_j(x)\,d\Gamma(x) + \sum_n \int_{L_n} U_{ij}(x', X)f_j^n(X)\,dL_n(X) \tag{2}$$

where the coefficient $c_{ij}(x')$ can be determined by rigid body movement considerations.

The corresponding tractions at boundary points x' are given by

$$c_{ij}(x')t_j(x') = -n_i(x')\int_\Gamma S_{ijk}(x', x)u_k(x)\,d\Gamma(x) + n_i(x')\int_\Gamma D_{ijk}(x', x)t_k(x)\,d\Gamma(x) + n_i(x')\sum_n \int_{L_n} D_{ijk}(x', X)f_k^n(X)\,dL_n(X) \tag{3}$$

where $S_{ijk}(x', x)$ and $D_{ijk}(x', x)$ contain derivatives of $T_{ij}(x', x)$ and $U_{ij}(x', x)$, respectively; $n_i(x')$ denotes the ith component of the unit outward normal to the boundary at the point x'; and the coefficient $c_{ij}(x')$ is equal to $\delta_{ij}/2$ on a smooth part of the boundary, where δ_{ij} denotes the Kronecker delta.

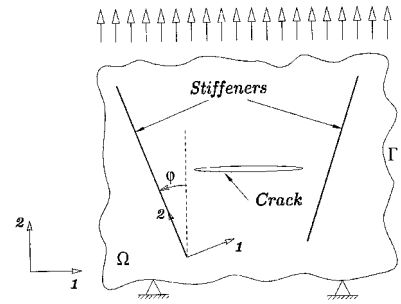

Fig. 1 Cracked stiffened sheet subjected to boundary tractions and displacement constraints.

If, in addition to the interaction forces $f_i(X)$, the stiffeners are subjected to concentrated in-plane loads $F_i(0)$ and $F_i(l)$ and in-plane moments $M(0)$ and $M(l)$, acting at both endpoints, their relative displacements (with respect to a rigid body motion of the starting point) in the 1) transverse and 2) longitudinal directions, are given by

$$v_1^n(y) = \frac{1}{A^nG^n}\left[yF_1^n(0) + \int_0^y (y-\eta)b_1^n(\eta)\,d\eta\right] - \frac{1}{I^nE^n}\left[\frac{1}{2}y^2M^n(0) + \frac{1}{6}y^3F_1^n(0) + \int_0^y \frac{1}{6}(y-\eta)^3b_1^n(\eta)\,d\eta\right] \tag{4}$$

$$v_2^n(y) = \frac{1}{A^nE^n}\left[yF_2^n(0) + \int_0^y (y-\eta)b_2^n(\eta)\,d\eta\right] \tag{5}$$

where b_i are the interaction forces expressed in the stiffeners coordinate system, y is an arc length parameter ($0 \le y \le l$), A is the cross-sectional area, I is the cross-sectional second moment of inertia, E and G are the stiffeners' material Young modulus and shear modulus, respectively.

The condition that the displacements u_i^s of the sheet and u_i^n at position y of the nth stiffener are compatible with the shear deformation of the adhesive layer connecting them is expressed by the following relation:

$$u_i^s - u_i^n = \phi^n\Delta f_i^n \tag{6}$$

where ϕ^n is the coefficient of shear deformation of the adhesive layer. The displacements u_i^n and the interaction forces f_i^n are expressed in the sheet coordinate system. They are related to v_i^n and b_i^n, respectively, by means of a coordinate system rotation defined by the angle ς^n between the sheet direction 2 and the nth stiffener axis (Fig. 1).

Equations (1–3) were developed for sheets with thickness $H = 1$. The effectiveness of a stiffener as a crack stopper depends on its relative stiffness with respect to the sheet, which, by its turn, depends on the thickness. To allow other values of H, it is necessary to multiply all integrals involving the attachment forces f_i in Eqs. (1–3) by $1/H$. That is, the influence of the stiffeners is scaled to have the correct relative stiffness.

If the boundary Γ and the stiffeners loci L_n are discretized into a set of boundary elements, a system of simultaneous linear equations can be constructed. There are two unknowns for each node at the boundary (two displacements or two tractions or one displacement and one traction depending on the boundary conditions prescribed for that node), and two unknowns for each node at the stiffeners loci (the interaction forces at each direction). The required number of equations can be obtained by applying Eq. (2) to the boundary nodes. If a crack is present, Eq. (3) is used instead of Eq. (2) when generating equations for nodes on one of the crack surfaces. This is necessary to avoid the generation of two identical equations for

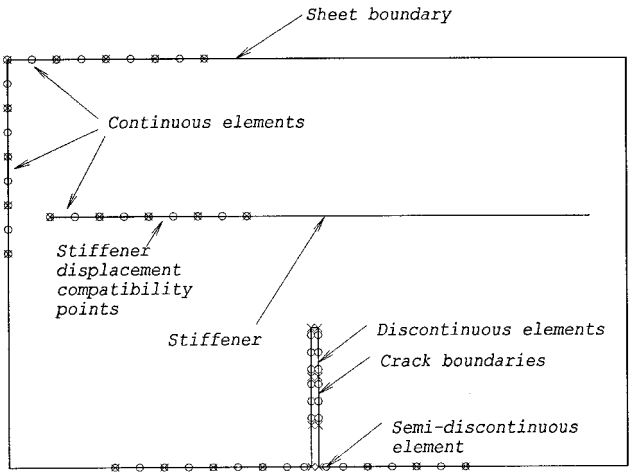

Fig. 2 Cracked stiffened sheet with indication of boundary elements used in the discretization. ○, node; ×, element endpoint; and +, internal point.

nodes at the crack surface. The use of traction Eq. (3) is the main distinguishing feature of the DBEM. For the nodes on each stiffener (with the exception of the reference nodes at $y = 0$), two displacement compatibility equations can be generated using Eqs. (1) and (4–6). There are still more unknowns than equations. The other necessary equations per stiffener can be constructed from the condition that the stiffeners are in equilibrium.

Figure 2 illustrates the discretization of the problem. Continuous quadratic elements are used to discretize the boundaries and the stiffeners loci, with the exception of the crack boundary where discontinuous quadratic elements are employed. This is necessary to properly integrate traction Eq. (3), which contains strongly singular terms. However, as will be seen later, the use of discontinuous elements at the crack boundaries has beneficial effects for the crack propagation analysis.

B. Discretely Attached Stiffeners

If the stiffeners are discretely attached to the sheet, i.e., by means of fasteners, instead of continuously distributed along the attachment lines, the interaction forces are considered as concentrated at points, corresponding to the fasteners positions, and the integrals over the stiffener elements in Equations (1–3) reduce to summations. That is

$$\sum_n \int_{L_n} (\text{kernel}) f^n(X)\, \mathrm{d}L_n(X)$$

reduces to

$$\sum_n \sum_{m_n} (\text{kernel}) f^{m_n}$$

where m_n stands for the nodes at the nth stiffener locus. In a similar manner, the integrals in Eqs. (4) and (5) also reduce to summations.

C. Attachment Models

Rigid attachments are modeled by specifying the attachment flexibility coefficient ϕ in Eq. (6) to be equal to zero. Linear elastic attachments are modeled by assigning ϕ as the proper flexibility value for the connection. Nonlinear attachment material behavior is taken into account according to the elastic–plastic force–deflection model illustrated in Fig. 3. If the attachment force f is below the limit $\bar{f}$, then the elastic flexibility is used. When $f > \bar{f}$, the attachment force at the point is set to $\bar{f}$, and the system is reanalyzed. Attachment failure caused by excessive deformation can be taken into account. When the limit deformation $\bar{d}$ is exceeded, the attachment force at the point is set to zero, and the system is reanalyzed. Convergence is achieved when all of the attachment forces and deformations are found to be within the specified limit.

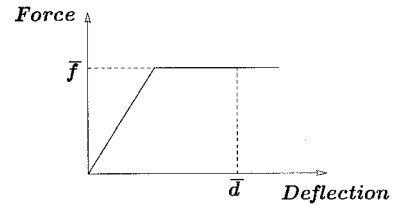

Fig. 3 Force-deflection model for elastic–plastic attachment behavior.

D. Evaluation of Stress Intensity Factors

Once the system of equations is assembled and solved for the unknown boundary displacements u_i, boundary tractions t_i, and interaction forces f_i, the stress intensity factors are calculated. Aliabadi and Rooke[5] describe different methods for the evaluation of stress intensity factors with BEM. Portela et al.[6] concluded that the J-integral technique is the best suited for the DBEM. A simple procedure, based on decomposition of the elastic field into its symmetric and antisymmetric modes, is used to decouple the J integral into mode I and II components. It can then be defined as

$$J^m = \int_S (W^m n_1 - t_j^m u_{j,1}^m)\, \mathrm{d}S \qquad m = I, II \tag{7}$$

where W is the strain energy per unit volume, n_1 is the component in direction 1 of the outward normal to the path S, t_j $(=\sigma_{ij} n_j)$ and u_j are the components of the interior tractions and displacements, respectively.

The J integral is related to the stress intensity factor; under plane stress conditions, the relationship is

$$J^I = \frac{K_I^2}{E} \quad \text{and} \quad J^{II} = \frac{K_{II}^2}{E} \tag{8}$$

E. Crack Growth Analysis

The direction of crack growth is calculated using the maximum principal stress criterion.[12] According to that criterion, crack growth will occur in a direction perpendicular to the maximum principal stress. The local crack-extension direction is determined by the condition that the shear stress at the crack tip is zero, that is,

$$K_I \sin\theta_t + K_{II}(3\cos\theta_t - 1) = 0 \tag{9}$$

where θ_t is an angular coordinate centered at the crack tip and measured from the crack axis ahead of the crack tip. However, the maximum principal stress criterion does not take into account the discreteness of the crack-extension modeling. Thus, the direction of the crack-extension increment must be corrected to take the size of the increment into account. A prediction–correction scheme[6] is adopted here.

In multiple-cracks problems, it is necessary to determine not only the direction of the crack extension, but also the relative sizes of the increments, i.e., the relative growth rates between the various crack tips. The fatigue crack growth properties of the structural material ($\mathrm{d}a/\mathrm{d}N$) are usually given as a function of the effective stress intensity factor range ΔK_{eff}. For the sake of simplicity, Paris law[13] is used. That is,

$$\frac{\mathrm{d}a}{\mathrm{d}N} = C(\Delta K_{\text{eff}})^m \tag{10}$$

where C and m are the Paris material parameters, and ΔK_{eff} is given by Tanaka[14] as

$$\Delta K_{\text{eff}}^2 = \Delta K_I^2 + 2\Delta K_{II}^2 \tag{11}$$

For constant amplitude fatigue load with stress amplitude ratio R, $\Delta K_I = K_I(1 - R)$ and $\Delta K_{II} = K_{II}(1 - R)$.

Crack-extension increment sizes are determined as follows:

First, the effective stress intensity factors are calculated and the crack growth Eq. (10) is integrated to determine, for each crack tip (i), the number of cycles (ΔN_i) necessary to grow an arbitrary reference size (RS):

$$\Delta N_i = \frac{1}{C}\int_{a_i}^{a_i+\text{RS}} \frac{1}{(\Delta K_{\text{eff}})^m}\,\mathrm{d}a \tag{12}$$

where the integration is performed assuming that the stress intensity factors remain constant as the crack grows from the initial size a_i to a_i + RS.

It is then assumed that the fast-growing crack tip, i.e., the one for which the smallest number of cycles [ΔNC = min(ΔN_i)] was calculated, will grow the predefined size RS. The increment sizes of the other cracks are then calculated by integrating the inverse of the crack-growth equation

$$\Delta a_i = C\int_{\text{NC}}^{\text{NC}+\Delta\text{NC}} (\Delta K_{\text{eff}})^m\,\mathrm{d}N \tag{13}$$

using the minimum number of cycles previously determined (ΔNC) to calculate the growth length. Again, the stress intensity factors are assumed to remain constant.

The boundary element mesh is then updated to include the new increments, and a structural analysis is performed, at the end of which new stress intensity factors are evaluated. The increments size is then recalculated, now taking into account the variation of the stress intensity factors when integrating Eqs. (12) and (13). The increments are remeshed and a new structural analysis is performed. This procedure is repeated until convergence for the increments size is achieved.

The increments direction and size are calculated simultaneously as summarized.

1) Perform structural analysis.

2) Calculate the effective stress intensity factors range.

3) Calculate the crack increments direction and size assuming that, as the cracks grow, the effective stress intensity factors range remains constant.

4) Update mesh to include the crack increments.

5) Perform new structural analysis.

6) Calculate new effective stress intensity factors range.

7) Correct the crack increments direction and size considering the variation of the stress intensity factors from their former to new values.

8) Verify convergence for the increments direction and size. If not achieved return to step 4.

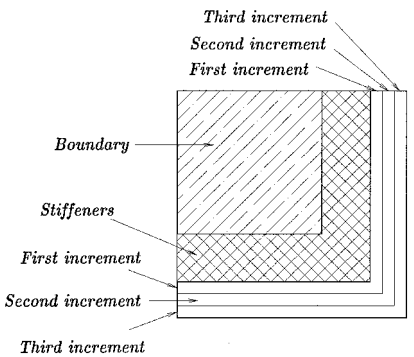

Fig. 4 System matrix arrangement.

Remeshing after each crack increment is reduced to adding new elements to the crack boundary. No change is required in the existing mesh. Moreover, because of the use of discontinuous elements at the crack boundaries, only matrix coefficients as a result of the new elements have to be calculated and added as new rows and columns to the existing (LU-decomposed) matrix. Only the new rows and columns have to be decomposed during the current increment, and the computational time is substantially reduced. Figure 4 illustrates the way in which each increment is added to the system matrix.

III. Test Examples

A. Crack Growth Rates in Stiffened Panels

Poe[15] calculated stress intensity factors in stiffened panels using a force-displacement matching technique. Later, he performed a comprehensive series of measurements of fatigue crack growth rates in stiffened panels.[16] Those results were used to assess the extent to which the stress intensity factors[15] could be used to predict crack growth rates in a stiffened panel. To calculate crack growth rates from the stress intensity factors, Poe[16] used the empirical equation for fatigue crack growth rate proposed by Forman et al.[17]

$$\frac{\mathrm{d}a}{\mathrm{d}N} = \frac{C(\Delta K)^n}{(1 - R)K_c - \Delta K} \tag{14}$$

where ΔK is the stress intensity factors range, and R is the stress ratio. The values of the critical stress intensity factor K_c and the constants C and n were determined by least-squares fit, from growth rates measured in unstiffened sheets made from the same material used in the test specimens.[16]

In this example, the technique introduced in the preceding sections is used to calculate the stress intensity factors for one of the panels studied by Poe.[16] Those stress intensity factors are then introduced in Eq. (14) to predict the crack growth rates, and results are compared with the experimental data available.

The panel chosen was constructed of 0.09-in.-thick aluminium alloy 2024T3 sheets, with Young's modulus equal to 10400 ksi and stringers spaced at 6.0 in. The stringers were made of aluminium alloy 2024T4, with Young's modulus 10700 ksi. The stiffeners cross-sectional area was 0.75 in.^{2} (0.375 $\times$ 2.0 in.). The stringers were bolted to the sheet with 1/4-in. aluminium alloy interference fit lock bolts. The fasteners pitch was 1 in. The panel was assembled with 11 stiffeners, and a starter notch 0.5 in. long was cut in the center of the panel each side of the central stiffener.

The panel was subjected to axial cyclic loading of constant amplitude. The sheet and the stiffeners were initially equally strained by the applied load. The maximum stress in the sheet was 15 ksi and the stress ratio was 0.1. The value of the coefficients in Eq. (14) are $C^1 = 6.85 \times 10^{-8}$ [in./(ksi$\sqrt{\text{in.}}$)$^{n-1}$], $K_c = 92$ (ksi$\sqrt{\text{in.}}$), and $n = 3.5$.

Crack growth rates for the panel were predicted with and without an allowance for attachment deflection, i.e., taking the flexibility of the attachment into account. In the second case, the attachment flexibility was calculated using the empirical equation derived by Swift[4]

$$q = \frac{1}{E_r d}\left[A + Bd\left(\frac{1}{H_{\text{stf}}} + \frac{1}{H}\right)\right] \tag{15}$$

where q is the attachment deflection caused by a unit load, E_r is the Young's modulus of the rivet, d is the rivet diameter, H_{stf} and H are the stiffener and sheet thicknesses, respectively. The value of the constants A (5.0) and B (0.8) were determined by Swift for aluminium fasteners.

The configuration studied is a rectangular sheet with a width of 36 in. and a height of 48 in., with five stiffeners equally spaced along the sheet width. Each stiffener contains a total

of 40 rivets with 20 rivets on either side of the crack line. Convergence was achieved with a boundary element mesh of 36 elements on the sheet boundary, 20 elements on each stiffener locus, and 2 elements on each of the crack surfaces. Using twice as many elements on the crack and sheet boundaries resulted in changes in the stress intensity factors of less than 0.7%. A crack propagation analysis was performed in which the crack was extended by 0.5-in. increments until the crack length a was equal to 9 in. Each crack extension was modeled with four additional elements, one on each crack surface at either crack tip.

Results are presented in Fig. 5. Each pair of curves was obtained by multiplying the results from Eq. (14) by 0.640 and 1.665, respectively. These constants were determined[16] and correspond to the 5th and 95th percentiles of the error that was minimized in the least-squares fit.

It can be seen that the results obtained for rigid attachments (without allowance for attachment deflection) show good agreement with the empirical values presented by Poe,[16] particularly when the crack tip is not beyond the first stiffener (a = 6 in.). The higher growth rates predicted by making an allowance for attachment deflection were not realized. A similar trend was observed by Cartwright and Dowrick.[18] The reason is that, in the panels tested by Poe,[16] the stiffener was fixed to the sheet with lock-bolts, which behave in a less flexible manner than the riveted joint on which Eq. (15) is based, especially at low levels of load. However, when the crack tip is near or beyond the stiffener, the results obtained with allowance for attachment deflection correctly predict that the stiffener is not as effective in reducing the stress intensity factor as indicated by the values calculated without taking the attachment flexibility into account.

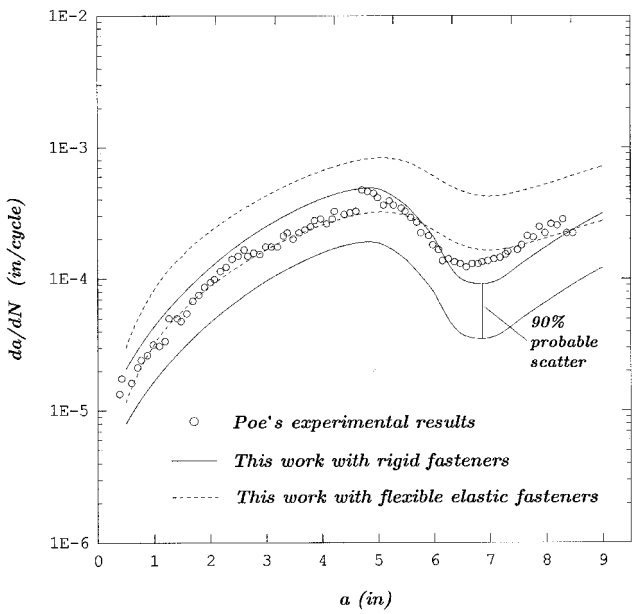

Fig. 5 Crack growth rates for stiffened panel (Poe's experimental data against predicted rates[16]).

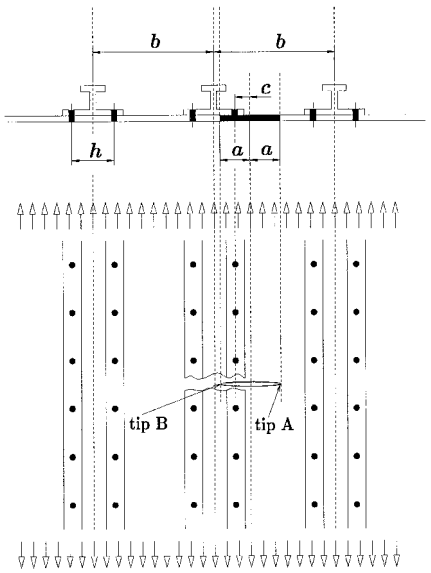

Fig. 6 Example proposed by Low and Cartwright[19] to study the effect of different attachment models.

B. Effect of Attachment Models

The effect of the different attachment models is demonstrated with the help of an example introduced by Low and Cartwright.[19] A typical wing skin panel as shown in Fig. 6 is subjected to a uniform tensile stress σ. The sheet is 18.4 mm thick. Young's modulus is 73,800 MPa, yield stress σ_y = 386 MPa, and Poisson's ratio 0.3. The I-section stiffeners have a cross-sectional area of 1710 mm^2 and a Young's modulus of 74,500 MPa, and are attached periodically to the sheet a distance b (185.4 mm) apart. Each of the stiffeners is attached to the sheet with a double row of fasteners of diameter 8 mm. The lateral fastener spacing between the double rows is h (58.4 mm) and the fastener pitch is 38.1 mm. The sheet contains a crack of length $2a$ (a = 47.6 mm). The center of the crack is at a distance c (19.7 mm) from the adjacent line of fasteners in the central stiffener (Fig. 6).

The doubly attached stiffeners are modeled as two independent stiffeners of area 855 mm^2 ($\frac{1}{2} \times$ 1710 mm^2). The central stiffener is assumed to be broken, and a total of 15 fasteners are modeled on either side of the crack line. The sheet boundary and the stiffener loci were discretized with 32 and 90 elements, respectively, and each of the crack surfaces with eight elements. Doubling the number of elements on the sheet and crack boundaries resulted in changes in the stress intensity factors of less than 0.5%.

The panel is analyzed with the fasteners modeled as either rigid or flexible (in the last case, with elastic or elastic–plastic behavior). Low and Cartwright[19] used a piecewise-linear representation of the attachment force–deflection curve. In their model, four linear segments were used to approximate the nonlinear material behavior. Table 1 and Fig. 7 present the parameters Low and Cartwright[19] used along with the parameters used in the more simple elastic–plastic representation adopted in this work.

Stress intensity factors calculated for tips A and B, for each of the attachment models, are presented in Fig. 8, normalized with respect to $K_0 = \sigma\sqrt{\pi a}$. Results show good agreement with values calculated by Low and Cartwright.[19] For rigid and flexible attachment with linear behavior, the differences are below 1%. For flexible attachment with elastic–plastic behavior, the differences are between 1 and 1.5% for σ/σ_y = 0.3 (tip B), 0.5 (tips A and B), and 0.9 (tip A), and below 1% for all of the other cases. The higher differences in those cases are a result of the different models adopted for the elastic–plastic behavior.

Table 1 Fastener piecewise linear force deflection curves parameters

d, mm	ϕ, 10^{-6} mm/N	f, N, Ref. 19	f (N), this work
0.0761	3.8	20,020	20,020
0.1521	10.2	27,470	30,000
0.3301	48.5	31,140	30,000
0.9266	372.8	32,740	30,000

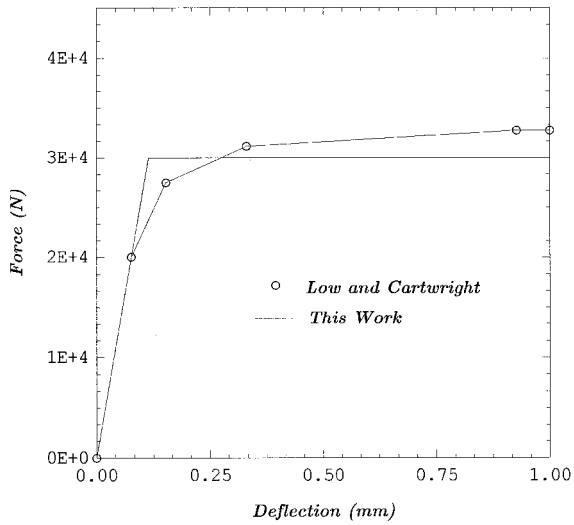

Fig. 7 Force deflection models for the panel with double row of fasteners.

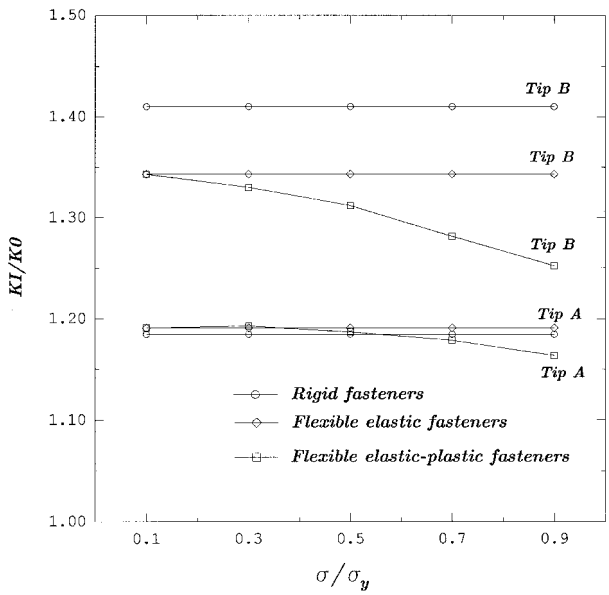

Fig. 8 Stress intensity factors for different attachment models ($K_o = \sigma\sqrt{\pi a}$).

C. Multiple Cracks in Stiffened Panel

Figure 9 presents a stiffened panel subjected to a uniform tensile stress. The sheet is 0.8 mm thick. It is made of aluminium alloy A2024T3 with Young's modulus 73,000 MPa and Poisson's ratio 0.32. The stiffeners have a cross-sectional area 160 mm^2 and are made of aluminium alloy A7475T761 with Young's modulus 69,000 MPa. They are attached periodically to the sheet a distance b (415 mm) apart with a single row of fasteners of diameter 4 mm and linear flexibility coefficient equal to 4.45×10^{-5} mm/N. The fasteners pitch is p (25 mm) and each stiffener is modeled with 24 fasteners. The sheet contains a crack of length $2a$ (a = 41.5 mm). The center of the crack is at the central fastener of the central stiffener. The aim of this example is to study the influence of cracks at adjacent stiffeners on the central crack. The central stiffener can be broken or intact. The lateral cracks have the same initial size as the central one and are considered either aligned with the central crack or misaligned. In the latter case, their axes are supposed to be initially parallel and a distance h apart as shown in Fig. 9. The panels were subjected to cyclic loading of constant amplitude with the maximum value of 50 MPa and stress ratio equal to zero. Equation (10) with $C = 0.183 \times 10^{-11}$ and $m = 3.284$ is used to calculate the crack growth rates. Crack propagation analysis was performed for the following configurations: 1) panel with intact central stiffener and central crack only; 2) panel with intact central stiffener and aligned lateral cracks ($h = 0$); 3) panel with intact central stiffener and misaligned cracks ($h = p$, $2p$, $3p$, $4p$); 4) panel with broken central stiffener and central crack only; 5) panel with broken central stiffener and aligned lateral cracks ($h = 0$).

The BEM mesh for the analysis of the panel with intact central stiffener and misaligned cracks ($h = p$, a = 41.5 mm) is presented in Fig. 10. Convergence was achieved with a total of 100 quadratic boundary elements, and the stress intensity factors varied less than 0.5% as the number of elements on the sheet and crack boundaries was doubled.

Stress intensity factors and number of loading cycles for the cases with the central stiffener intact are presented in Figs. 11 and 12, respectively. The results are for the tips in the central crack and are normalized with respect to corresponding values

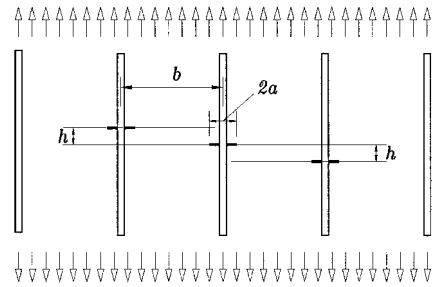

Fig. 9 Stiffened panel with multiple cracks.

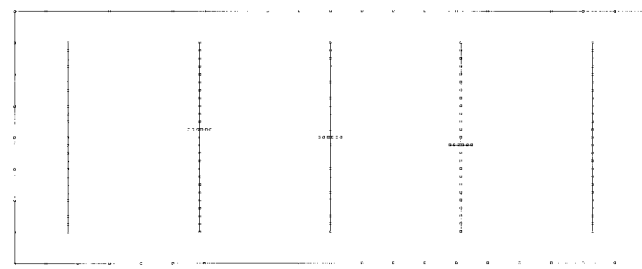

Fig. 10 Boundary element mesh for stiffened panel with multiple cracks and intact central stiffener.

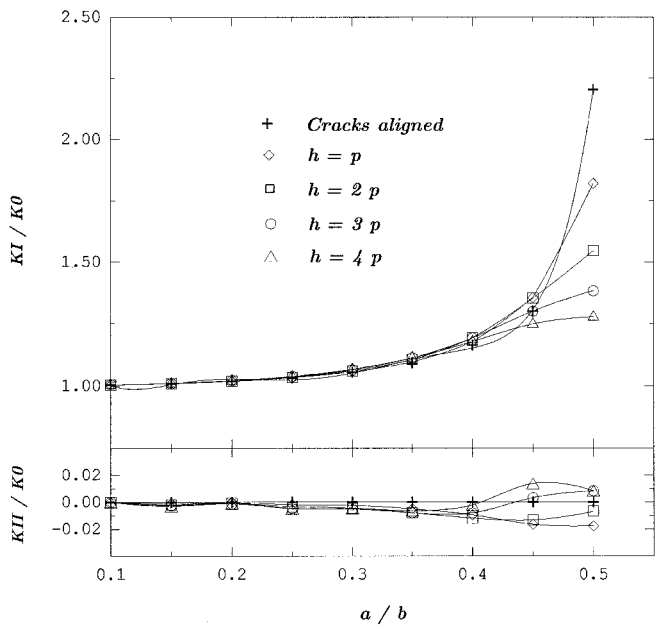

Fig. 11 Stress intensity factors for a panel with multiple cracks and intact central stiffener.

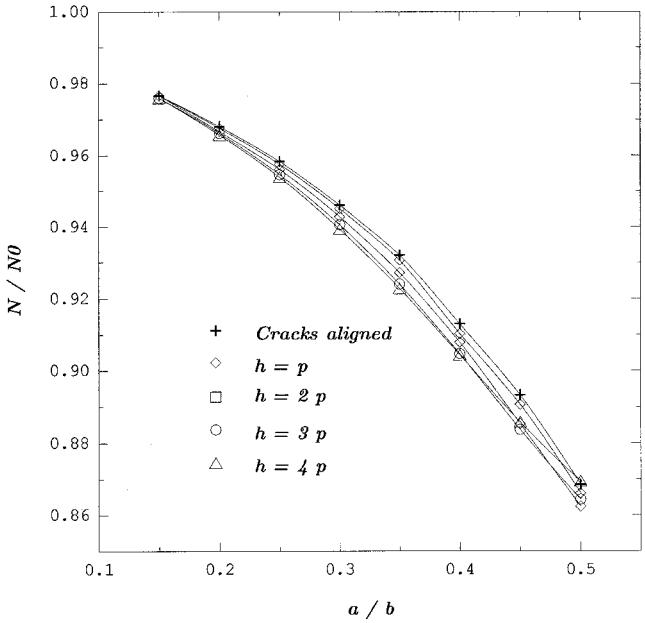

Fig. 12 Number of cycles for a panel with multiple cracks and intact central stiffener.

(mode $I = 0.02$ s^{-1} stress intensity factors and number of cycles) calculated for the configuration with central crack only (case 1). The analysis was extended to values of a/b up to 0.5. That is possible because the crack tips in the lateral cracks grow at slightly lower rates than the ones in the central crack. However, one should be aware that because of the reduction of the sheet net section, high stresses can develop in the region, leading to link-up of the tips or plasticity. It can be seen in Fig. 11 that for all cases, the mode I stress intensity factors are higher than for the case without the lateral cracks (case 1), and that the critical case is the one with the cracks aligned. As distance h increases, the influence of the lateral cracks is reduced. Mode II stress intensity factors are very small in comparison with their mode I counterparts. That is to be expected because of the mode I nature of the loading and to the adoption of the principal stress criterion for the calculation of the crack increments direction, i.e., the growth direction is chosen to minimize K_{II}. It can be seen in Fig. 12 that for all cases the number of cycles required for the crack to grow is slightly less than for the case without the lateral cracks (case 1) and that the distance between the cracks axis (h) does not seem to be significant. It can be concluded that the presence of cracks under adjacent stiffeners has a more important effect on the residual strength than on the fatigue life. It is safe to use the pure mode I case (with the cracks aligned) to analyze configurations such as the ones presented in this example.

A broken central stiffener considerably overloads the central crack.[20] The effect of the overload is to make the growth rates for the tips in the central crack much higher then the ones for the tips in the lateral cracks. Thus, the growth of the tips in the lateral cracks is rendered negligible. The analysis was performed for cases 4 and 5 and extended to values of a/b up to 0.8. The same observations as made in the preceding text, with respect to the net section stress level, apply. Results are presented in Fig. 13, where mode I stress intensity factors for case 5 are normalized with respect to the values for case 4. The number of required loading cycles was found not to be affected by the presence of the lateral cracks in case 5.

D. Multisite Damage in Lap Joint Splice

Inspection of aging transport aircraft have shown that multisite damage (MSD) (a large colony of similar cracks at adjacent rivet holes) can occur. The consequence of undetected MSD was dramatically demonstrated when a Boeing 737 aircraft lap joint failed in flight in April 1988. Since then, a great deal of effort has been devoted to the analysis of such problems. This example illustrates how the technique proposed here can be used to study the crack growth process in lap joints.

Figure 14 presents a segment of a lap joint subjected to a uniform tensile stress equal to 62.5 MPa. The sheet is 1.0 mm thick. Its material is aluminium alloy A2024T3 with Young's modulus 73,000 MPa and Poisson's ratio 0.32. The main dimensions are presented in Fig. 14 as a function of the rivet hole diameter r (2 mm). Seven cracks are emanating from the rivet holes in the upper row. Cracks 1, 3, 5, 6, and 7 have an initial size of $r/4$, whereas cracks 2 and 4 have an initial size of $r/2$.

The following strategy was used to study this problem. Initially, one analysis was performed, in which the cracks were removed and the tensile stress was applied at the top edge of the sheet model. Displacement boundary conditions were introduced to the lower half of the rivet holes to simulate frictionless rigid pins. The aim of this analysis was to obtain an approximation to the stress distribution at the rivet holes' surface. A second analysis was then performed, using the calcu-

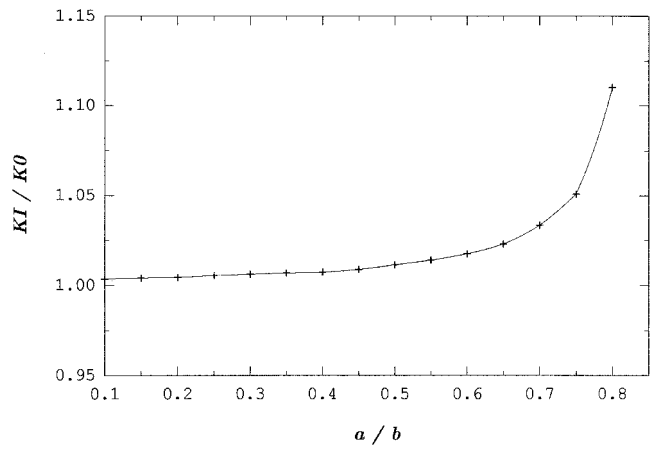

Fig. 13 Stress intensity factors for a panel with multiple cracks and broken central stiffener.

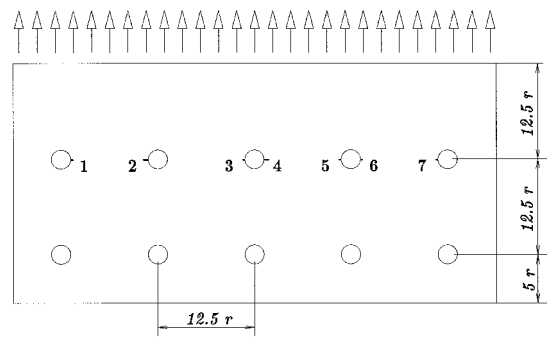

Fig. 14 Multiple site damage problem in fuselage lap joint splice.

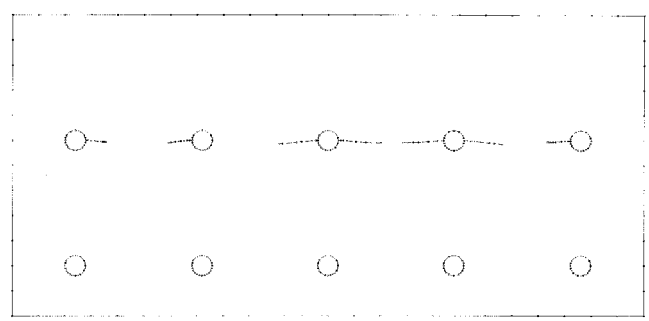

Fig. 15 Boundary element mesh and crack paths for lap joint problem.

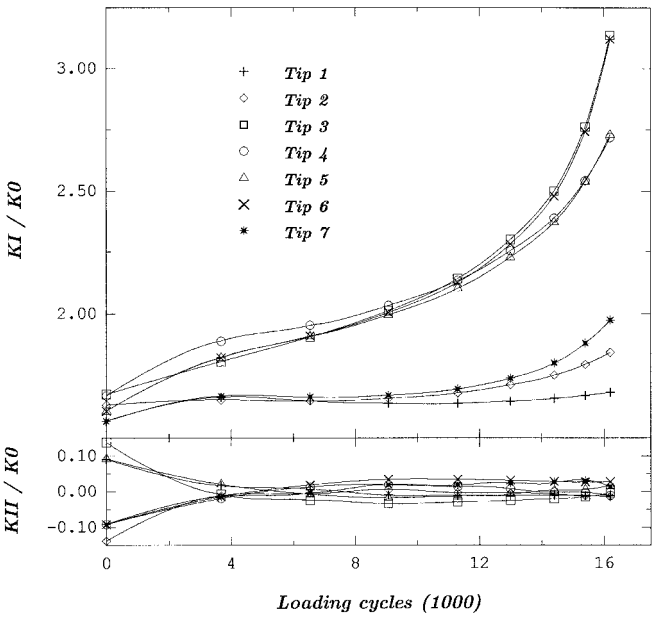

Fig. 16 Stress intensity factors for the lap joint problem ($K_0 = \sigma\sqrt{\pi r}$).

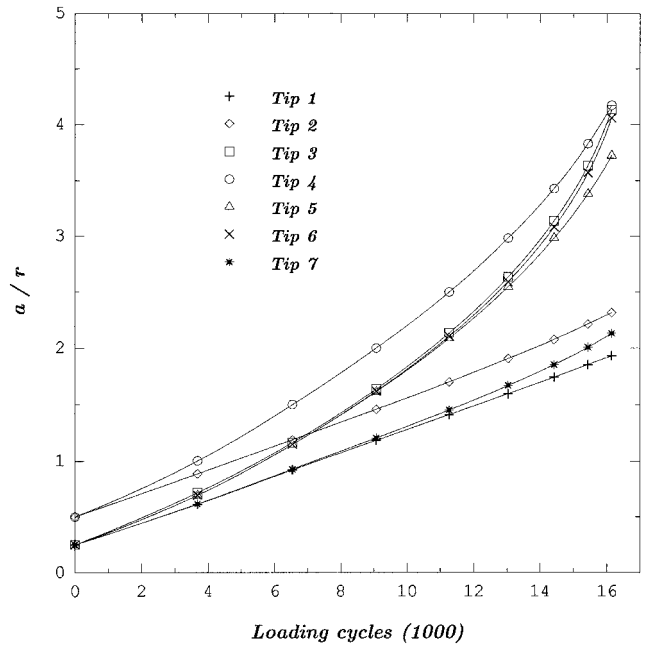

Fig. 17 Crack growth diagram for lap joint problem. Results normalized with respect to the rivet hole radius *r*.

lated stress distribution at the rivet holes' surface and introducing displacement boundary conditions at the top edge of the sheet model. The normal reaction forces obtained at the top edge of the sheet were then compared with the original value of the uniform tensile stress (62.5 MPa) and found to be in good agreement. The cracks were then introduced in the later model and a crack propagation analysis was performed. The joint was submitted to cyclic loading of constant amplitude and a stress ratio equal to zero. Equation (10), with $C = 0.183 \times 10^{-11}$ mm/(N$\sqrt{\text{mm}}$)^m and m = 3.284, was used to calculate the crack growth rates.

The BEM mesh and the resulting crack paths are presented in Fig. 15. Each rivet hole was discretized with 10 elements and the cracks with one element on either crack surface. Each increment of the crack extension process was modeled with the addition of two elements to each crack, one element on either crack surface.

The stress intensity factors are presented in Fig. 16 normalized with respect to $K_0 = \sigma\sqrt{\pi r}$. The crack growth diagram is presented in Fig. 17 normalized with respect to the rivet hole radius *r*. It can be seen that despite the initial size, the cracks that start at rivet holes that are cracked at both sides tend to grow to a similar size prior to link-up. The analysis was later repeated using the model with the tension loads applied at the top edge and displacement boundary condition simulating a frictionless rigid pin applied at the rivet holes. The results were found to be remarkably similar to those presented in Figs. 15–17.

Conclusions

In this paper, the application of the DBEM to crack propagation analysis of aircraft-stiffened panels is demonstrated. The basic equations of the DBEM were presented. It was shown how displacement compatibility, imposed at the internal attachment points, can be used to introduce the stiffeners in the formulation. The resulting system is a powerful numerical tool, capable of performing crack propagation analysis in mixed mode problems involving single or multiple cracks, with any number of stiffeners (intact or broken). Bonded, riveted, and integral stiffeners are included. The stiffeners attachment can be rigid or flexible, with elastic or elastic–plastic behavior. Partial attachment failure can be simulated. Crack growth rates calculated from stress intensity factors obtained with the method were shown to be in good agreement with experimental results. Several damage tolerance analysis problems for typical aircraft-stiffened panels were presented, demonstrating the accuracy and flexibility of the technique. An example was presented illustrating the ability of the system to analyze MSD problems in lap joints.

The system described here is the core of an object-oriented damage tolerance design environment currently under development. The environment was conceived to support the engineer from the creation of the DBEM model to the preparation of the residual strength and crack growth diagrams, including the generation of the BEM mesh and the numerical analysis. It provides a high level of abstraction, allowing the engineer to concentrate on the design problem rather than on the details of the numerical model. All of the examples presented here were prepared and analyzed with the help of that environment using a personal computer.

Acknowledgments

This work was sponsored by Conselho Nacional de Desenvolvimento Científico e Tecnológico and Empresa Brasileira de Aeronáutica S.A. The authors express their appreciation to F. Fontana and D. J. Cartwright for the fruitful discussions.

References

[1]Viegler, H., "The Residual Strength Characteristics of Stiffened Panels Containing Fatigue Cracks," *Engineering Fracture Mechanics*, Vol. 5, No. 2, 1973, pp. 447–477.

[2]Ratwani, M. N., and Wilhem, D. P., "Influence of Biaxial Loading on the Analysis of Cracked Stiffened Panels," *Engineering Fracture Mechanics*, Vol. 11, No. 3, 1979, pp. 585–593.

[3]Shkarayev, S. V., and Moyer, E. T., "Edge Cracks in Stiffened Plates," *Engineering Fracture Mechanics*, Vol. 27, No. 2, 1987, pp. 127–134.

[4]Swift, T., "The Effects of Fastener Flexibility and Stiffener Geometry on the Stress Intensity in Stiffened Cracked Sheets," *Proceedings of the Conference on Prospects of Fracture Mechanics*, edited by G. C. Sih, H. C. von Elst, and D. Broek, Noordhoff International, Leyden, The Netherlands, 1975, pp. 419–457.

[5]Aliabadi, M. H., and Rooke, D. P., *Numerical Fracture Mechanics. Computational Mechanics Publications*, Southampton and Kluwer Academic Publishers, Dordrecht, The Netherlands, 1991.

[6]Portela, A., Aliabadi, M. H., and Rooke, D. P., "The Dual Boundary Element Incremental Analysis of Crack Propagation," *Computers and Structures*, Vol. 46, No. 2, 1993, pp. 237–247.

[7]Dowrick, G., Cartwright, D. J., and Rooke, D. P., "Boundary Ef-

fects for a Reinforced Cracked Sheet Using the Boundary Element Method," *Theoretical and Applied Fracture Mechanics*, Vol. 12, No. 3, 1990, pp. 251–260.

[8]Young, A., Rooke, D. P., and Cartwright, D. J., "Analysis of Patched and Stiffened Cracked Panels Using the Boundary Element Method," *International Journal of Solids and Structures*, Vol. 29, No. 17, 1992, pp. 2201–2216.

[9]Utukuri, M., and Cartwright, D. J., "Stress Intensity Factors for a Crack near Finite Boundaries in Multiply Stiffened Sheets," *Theoretical and Applied Fracture Mechanics*, Vol. 15, No. 3, 1991, pp. 257–266.

[10]Wu, B., and Cartwright, D. J., "The Boundary Collocation Method for Stress Intensity Factors of Cracks at Internal Boundaries in a Multiply Stiffened Sheet," 3rd Int. Conf. on Localized Damage, Computer Aided Assessment and Control, Udine, Italy, June 1994.

[11]Salgado, N. K., and Aliabadi, M. H., "The Application of the Dual Boundary Element Method to the Analysis of Cracked Stiffened Panels," *Engineering Fracture Mechanics*, Vol. 54, No. 1, 1996, pp. 91–105.

[12]Erdogan, F., and Sih, G. C., "On Crack Extension in Plates Under Plane Loading and Transverse Shear," *Journal of Basic Engineering*, Vol. 85, 1963, pp. 519–527.

[13]Paris, P. C., "The growth of fatigue cracks due to variations in load," PhD. Dissertation, Lehigh Univ., Bethlehem, PA, 1962.

[14]Tanaka, K., "Fatigue Crack Propagation from a Crack Inclined to the Cyclic Tensile Axis," *Engineering Fracture Mechanics*, Vol. 6, 1974, pp. 493–507.

[15]Poe, C. C., "Stress-Intensity Factor for a Cracked Sheet with Riveted and Uniformly Spaced Stringers," NASA TR R-358, May 1971.

[16]Poe, C. C., *Fatigue Crack Propagation in Stiffened Panels, Damage Tolerance in Aircraft Structures*, American Society for Testing and Materials, STP 486, 1971, pp. 79–97.

[17]Forman, R. G., Kearny, V. E., and Engle, R. M., "Numerical Analysis of Crack Propagation in Cyclic-Loaded Structures," *Journal of Basic Engineering, ASME Transactions, Series D*, Vol. 89, Sept. 1967, pp. 459–464.

[18]Cartwright, D. J., and Dowrick, G., *Effects of Attachment Deflection on Fatigue Crack Growth Rate in a Stiffened Sheet, Fracture Mechanics in Engineering Practice*, edited by P. Stanley, Applied Science Publications, London, 1977, pp. 361–372.

[19]Low, M. C., and Cartwright, D. J., "Fracture Diagrams for Stiffened Aircraft Structures: Effect of Material Non-Linearity," *Proceedings of the 13th Symposium on Aeronautical Fatigue* (Pisa, Italy), edited by A. Salvetti and G. Cavallini, EMAS, Ltd., Surrey, London, UK, 1985, pp. 551–583.

[20]Salgado, N. K., and Aliabadi, M. H., "Stress Intensity Factors for a Crack near Broken/Intact Stiffener," *International Journal of Fracture*, Vol. 74, No. 4, 1996, pp. R71–R74.